Evaluating the Interior Ballistic Performance of a Gun with a Gas-operated Piston System

Yanhui Jiang

School of Mechanical Engineering, Nanjing University of Science and Technology;
Xuanwu, Nanjing, 210094, China

Email: jyhnl@njust.edu.cn

Abstract

While the subject of ballistics has been investigated for several centuries, nowadays, the design of a ballistic component or device is still not an easy task, but usually a process of trial and error, or an iterative process of analysis, testing and tweaking. Concerning the design of a gun with a gas-operated piston system, it is challenging to accurately determine how a gas-operated piston system would affect the interior ballistic performance of the gun (e.g., muzzle velocity) due to gas loss and how large the chamber/gas-room pressure would be for safety purpose. To address this problem, a numerical approach based on the coupled Euler-Lagrange technique and a constitutive model for the combustion gas mixture of solid propellants is presented, where the constitutive model is developed by combining Vieille's law for combustion and the equation of state for gas mixture. The model is validated by experiments for a double base propellant. The approach is then applied to study the effect of a gas-operated piston system on the interior ballistic performance of typical gun designs with different gas port radiuses. The interior ballistic parameters like the muzzle velocity and the highest barrel pressure are computed. Results show that these designs of gas ports influence the interior ballistic parameters very little. In addition, a larger gas port radius results in a larger gas room pressure, which indicates a faster operation of the gas-operated piston.

Keywords: Interior ballistics; Finite element analysis; Constitutive modeling; Combustion; Fluid solid interaction

1. Introduction

Gas-operated piston systems are widely adopted in modern gun design to realize automatic cartridge unloading. Concerning the design of a gun with a gas-operated piston system, it is challenging to accurately determine how a gas-operated piston system would affect the interior ballistic performance of the gun (e.g., muzzle velocity) due to gas loss and how large the chamber/gas-room pressure would be for different gas port design(e.g., inclined angle and size).

While performing experiments is a direct approach to evaluate the design of a gun with a gas-operated piston system, it is usually expensive and even sometimes impossible. Thus, direct experiments are not suitable for the initial design phase of conceptual design. In contrast, an efficient numerical approach is preferred at this stage. In this paper, as an example, a digital model of a gun with a gas-operated system is presented. To evaluate its interior ballistic performance, a numerical approach based on coupled Euler-Lagrange (CEL) technique and a constitutive modeling for the combustion gas mixture of solid propellants is also presented. In the approach, the constitutive model is developed by combining Vieille's law for combustion and the equation of state for gas mixture in the context of two-scale homogenization of continuum. In addition, a method to estimate the material parameters for the constitutive model is proposed based on chemical reaction formula of solid propellants, e.g., double base propellant.

Since the mid-18th century, mathematical modeling and analysis of interior ballistic process has started aiding in gun design [1], e.g., the law of pressure determined by Hutton and Arcy, the equation of state for propellant gas derived by Rumford, Nobel and Abel. Nevertheless, the design of an interior ballistic component or device is still not an easy task to date, but usually an iterative process of trial and error [2-5]. Nowadays, one can find many refined lumped parameter models developed to predict interior ballistic parameters of various gun designs, e.g., muzzle velocity and chamber pressure. Among these lumped parameter models, the well-known are the IBVHG2 model [6], the ARL-NGEN3 model [7], the Mobidic-NG model[8], the XKTC model [9], the SNL model [10], etc. All these models build up equations of motion for the projectile in terms of ordinary differential equations (ODEs) derived from the conservation laws (mass, momentum, and energy), and further identify the lumped parameters that characterize the propellant, gun and projectile. While these models are useful to estimate basic ballistic parameters for conceptual design purpose, they fail when detailed ballistic component or device has a complex geometric design where the interaction with the propellant combustion gas has to be considered, e.g., a barrel with a short/long stroke gas-operated piston system. Thus, one might resort to other modeling and analysis approaches, e.g., finite element method (FEM) [11-13], discrete element method (DEM) [14], and finite volume method (FVM) [15, 16]. These approaches are suitable for complex field

problems governed by partial differential equations (PDEs). To apply these approaches in the modeling and simulation of interior ballistic process, a reasonable consideration of the fluid-solid interaction (FSI) between the propellant gas and the solid parts (e.g., barrel and projectile) is the key problem. The techniques to solve this problem are generally classified into two categories: pure Lagrange techniques and Euler-Lagrange techniques. For pure Lagrange techniques, both solids and fluids are discretized by Lagrange meshes or particles, e.g., the moving mesh technique[17, 18] and the mesh free technique[19, 20]. For Euler-Lagrange techniques, the motion of fluids is resolved into Euler meshes that are fixed in space, thus, an interface to transfer field information between the Euler meshes for fluids and the Lagrange meshes for solids is necessary, e.g., the coupled Euler-Lagrange (CEL) technique (volume-of-fluid method based on Lagrange plus remap formulation) [21, 22] and the Co-simulation technique [23, 24]. Generally speaking, in terms of computation, Euler-Lagrange techniques are more accurate than pure Lagrange techniques, while more computationally expensive.

The rest of the paper is organized as follows. **Section 2** introduces the constitutive modeling of the combustion gas mixture of solid propellants. **Section 3** presents the interior ballistic simulation of a gun with a gas-operated piston system. Concluding remarks are given in **Section 4**.

2. Constitutive modeling of the combustion gas mixture of a double base propellant

The basic equations in continuum mechanics are briefly reviewed at first. For an arbitrary particle inside a continuum body with an initial configuration Ω_0, its position is denoted as $\mathbf{X}$. When the body deforms into a new configuration Ω_t subjected to external loads at time t, the particle would move to a new position $\mathbf{x}=\hat{\mathbf{x}}(\mathbf{X},t)$ with a velocity $\mathbf{v}=\hat{\mathbf{v}}(\mathbf{X},t)$. The classical field theory asserts that the motion of a continuum media should obey conservation laws (i.e., mass conservation, momentum conservation and energy conservation). [25]

$$\begin{cases} \dot{\rho}+\rho\nabla\cdot\mathbf{v}=0 \\ \rho\dot{\mathbf{v}}=-\nabla p+\nabla\cdot\boldsymbol{\tau}+\mathbf{f} \\ \rho\dot{e}=-p\nabla\cdot\mathbf{v}+\boldsymbol{\tau}:\nabla\mathbf{v}-\nabla\cdot\mathbf{q} \end{cases} \tag{1}$$

where ρ is the density, p is the pressure, $\boldsymbol{\tau}$ is the 2nd order symmetric deviatoric stress tensor, $\mathbf{f}$ is the prescribed body force, e is the specific internal energy, and $\mathbf{q}$ is the heat flux density. Since there are three independent governing field equations corresponding to three unknown field variables (i.e., density ρ, temperature T, velocity $\mathbf{v}$), additional constitutive equations are required to make the system closed. The general forms of these constitutive equations could be stated as

$$\begin{cases} \boldsymbol{\tau}=\hat{\boldsymbol{\tau}}(\rho,T,\mathbf{x},\mathbf{v}) \\ \mathbf{q}=\hat{\mathbf{q}}(\rho,T) \\ p=\hat{p}(\rho,T) \\ e=\hat{e}(\rho,T) \end{cases} \tag{2}$$

Their specific forms could be defined either by a micro-scale modeling approach according to material micro-mechanisms and thermodynamics, or by fitting experimental

data to a mathematical model that obeys the 2nd law of thermodynamics.

In a gun design, the commonly-used structural materials are steel, copper and engineering plastics. Their constitutive equations and material parameters are well-known (e.g., elasticity, plasticity, thermal expansion coefficient, thermal conductivity, specific heat), which could be readily looked up in a design booklet for simulation purpose. However, the constitutive model accounting for the combustion gas mixture of a solid propellant is rare. In this section, we present a constitutive modeling of the combustion gas mixture (i.e., an equation of state for a continuum mixture flow of gas and solid phase) in the context of continuum mechanics, where an adiabatic condition is assumed.

2.1 Vieille's law for combustion

We start with the closed bomb model for combustion, where a parameter called Web fraction f_{web} is introduced. It is defined as the ratio between the current characteristic diameter d_{web} of the solid propellant grains and its initial diameter D_{web}

$$d_{web}(t) = D_{web} f_{web}(t) \tag{3}$$

where the following equations hold $f_{web}(0) = 1$ and $f_{web}(t_b) = 0$, where t_b denotes the burn out time. Thus, the fraction of the burn out propellant could be expressed by the propellant fraction function (PFF) as

$$\phi = 1 - f_{web} \tag{4}$$

To account for the shape effect of propellant grains, a shape parameter θ, that

determines if the burning surface will be decreased, increased or unchanged as the burning proceeds, is usually introduced to modify the PFF as

$$\phi = (1 - f_{web})(1 + \theta f_{web}) \tag{5}$$

where $\theta > 0$ represents a digressive burning, $\theta < 0$ a progressive burning, and $\theta = 0$ a neutral burning.

In addition, the burning rate of the characteristic diameter could be described by the Vieille's law [26]

$$\frac{d}{dt}(d_{web}) = D_{web}\frac{df_{web}}{dt} = -\beta p^{\alpha} \tag{6}$$

where p is pressure, α is the burning rate index, and β is the burning rate coefficient, which could be determined by experiments. Combining Eq. (5) and Eq. (6) results in

$$\boxed{\frac{d\phi}{dt} = \frac{\beta\sqrt{(1+\theta)^2 - 4\theta\phi}}{D_{web}} p^{\alpha}} \tag{7}$$

2.2 Equation of state for a combustion gas mixture

To get started, we consider a representative volume element (RVE) with an initial volume V_0 and assume the RVE is full of spherical solid propellant grains, which are of the same diameter D_{web}. The total mass of RVE is evaluated as

$$m_s = \rho_s V_s = \rho_s \eta V_0 \tag{8}$$

where ρ_s is the density of the solid propellant, V_s is the volume of the solid propellant, and η is the volume fraction of the solid propellant

$$\eta = \frac{4}{24}\pi D_{web}^3 / D_{web}^3 = 0.5236 \tag{9}$$

Therefore, the initial average density of the RVE is

$$\rho_0 = \frac{m_s}{V_0} = \rho_s \eta \tag{10}$$

When combustion starts, the mass of the burn out solid propellant is determined by the PFF as

$$m_g = \phi m_s \tag{11}$$

which is equal to the mass of the burning-generated gas mixture due to mass conservation. We assume the volume V of the RVE expands at a constant pressure, the volume of the gas mixture is thus evaluated as

$$V_g = V - (1-\phi)\eta V_0 \tag{12}$$

The average density of the RVE would correspondingly change as

$$\rho = \frac{m_s}{V} \tag{13}$$

We further consider the released energy $E_{Chemical}$ inside the RVE due to chemical reactions and assume the energy is totally absorbed by the gas mixture without any dissipation. According to the 1st law of thermodynamics, the energy absorbed by the gas mixture turns into its internal energy

$$E_{Chemical} = m_g \overline{c}_{vmix} (T_a - T_0) \tag{14}$$

where $\overline{c}_{vmix}$ is the mean specific heat of the gas mixture at constant volume, T_0 is the initial ambient temperature, and T_a is the adiabatic flame temperature (i.e., the highest

temperature that the gas mixture can reach). Most experimental and computational evidences have shown that the temperature of the propellant gas during burning usually varies slightly. [27-29]. Thus, the adiabatic flame temperature is assumed as a constant. In addition, we assume the pressure p_g and temperature T_a of the gas mixture are related by an equation of state as

$$p_g V_g = m_g R_{mix} T_a \tag{15}$$

where R_{mix} is the specific gas constant of the gas mixture.

From Eq. (8), Eq. (11), Eq. (12), Eq. (14) and Eq. (15), one has

$$T_a = T_0 + \frac{Q}{\bar{c}_{vmix}} \tag{16}$$

and

$$p_g = \frac{\phi}{J-(1-\phi)\eta}\rho_0 R_{mix} T_a \tag{17}$$

where $Q = E_{Chemical}/m_g$ is the specific reaction heat and $J = V/V_0 = \rho_0/\rho$ is the volume ratio.

The average pressure of the RVE is derived according to the principle of work equivalence

$$\boxed{p = \frac{p_g V_g}{V} = p_g \frac{J-\eta(1-\phi)}{J} = \phi\rho R_{mix} T_a} \tag{18}$$

From Eq. (18), we see that the gas mixture behaves like an ideal gas at a constant temperature T_a when combustion is done (i.e., $\phi = 1$). By homogenization, the mixture

of the gaseous products and remaining solid DBP are deemed as a uniform continuum.

2.3 Estimation of the material parameters of a double base propellant

Consider the widely-used double base propellant (DBP)[30, 31], which is composed of 85% nitrocellulose (NC) and 15% Nitro-glycerin (NG) in mole percent. The grains are of the same size (i.e., $D_{web} \sim 550\mu m$) and of the same spherical shape (i.e., $\theta = 1$). Its chemical reaction formula is given as

$$\begin{aligned} &17C_{24}H_{30}\left(NO_2\right)_{10}O_{20} + 3C_3H_5\left(NO_3\right)_3 \\ &\rightarrow 250CO_2 + 167CO + 40H_2O + 222.5H_2 + 89.5N_2 + 1000\text{cal/g} \end{aligned} \tag{19}$$

According to this formula, the parameters ρ_s, R_{mix}, and T_a could be theoretically estimated as following. The stoichiometric coefficients could be listed by inspection

$$\begin{aligned} v_{NC} &= -17 \\ v_{NG} &= -3 \\ v_{CO_2} &= 250 \\ v_{CO} &= 167 \\ v_{H_2O} &= 40 \\ v_{H_2} &= 222.5 \\ v_{N_2} &= 89.5 \end{aligned} \tag{20}$$

The mole mass (g/mol) for each component is calculated as

$$\begin{aligned} M_{NC} &= 1098 \\ M_{NG} &= 227 \\ M_{CO_2} &= 44 \\ M_{CO} &= 28 \\ M_{H_2O} &= 18 \\ M_{H_2} &= 2 \\ M_{N_2} &= 28 \end{aligned} \tag{21}$$

Then, the initial mass fraction of reactants could be calculated

$$\begin{aligned} c_{NC} &= 0.9648 = 17 \times M_{NC} / \left(17 \times M_{NC} + 3 \times M_{NG}\right) \\ c_{NG} &= 0.0352 = 3 \times M_{NG} / \left(17 \times M_{NC} + 3 \times M_{NG}\right) \\ c_{CO_2} &= 0 \\ c_{CO} &= 0 \\ c_{H_2O} &= 0 \\ c_{H_2} &= 0 \\ c_{N_2} &= 0 \end{aligned} \tag{22}$$

The equilibrium mass fraction for each component is calculated according to the equation of atom number conservation and the reaction complete condition $c_{NC}^{*} = 0$ [32]

$$\begin{aligned} &\frac{c_{NC}^{*} - c_{NC}}{M_{NC} v_{NC}} \\ &= \frac{c_{NG}^{*} - c_{NG}}{M_{NG} v_{NG}} = \frac{c_{CO_2}^{*} - c_{CO_2}}{M_{CO_2} v_{CO_2}} = \frac{c_{CO}^{*} - c_{CO}}{M_{CO} v_{CO}} = \frac{c_{H_2O}^{*} - c_{H_2O}}{M_{H_2O} v_{H_2O}} = \frac{c_{H_2}^{*} - c_{H_2}}{M_{H_2} v_{H_2}} = \frac{c_{N_2}^{*} - c_{N_2}}{M_{N_2} v_{N_2}} \end{aligned} \tag{23}$$

Therefore, the explicit results could be written as

$$
\begin{aligned}
c^*_{NG} &= c_{NG} - \frac{M_{NG}}{M_{NC}}\frac{v_{NG}}{v_{NC}}c_{NC} = 0 \\
c^*_{CO_2} &= c_{CO_2} - \frac{M_{CO_2}}{M_{NC}}\frac{v_{CO_2}}{v_{NC}}c_{NC} = 0.5686 \\
c^*_{CO} &= c_{CO} - \frac{M_{CO}}{M_{NC}}\frac{v_{CO}}{v_{NC}}c_{NC} = 0.2417 \\
c^*_{H_2O} &= c_{H_2O} - \frac{M_{H_2O}}{M_{NC}}\frac{v_{H_2O}}{v_{NC}}c_{NC} = 0.0372 \\
c^*_{H_2} &= c_{H_2} - \frac{M_{H_2}}{M_{NC}}\frac{v_{H_2}}{v_{NC}}c_{NC} = 0.023 \\
c^*_{N_2} &= c_{N_2} - \frac{M_{N_2}}{M_{NC}}\frac{v_{N_2}}{v_{NC}}c_{NC} = 0.1295
\end{aligned}
\tag{24}
$$

Before the chemical reaction, the mass fraction of NC and NG are 0.9648 and 0.0352 respectively. Given the density of NC ρ_{NC}=1.66g/cm^3 and NG ρ_{NG}=1.26g/cm^3, the density of the DBP ρ_s could be derived as

$$
\boxed{\begin{aligned}
&\frac{1}{\rho_s} = \frac{0.9648}{\rho_{NC}} + \frac{0.0352}{\rho_{NG}} \\
&\Rightarrow \\
&\rho_s = 1.64\,g/cm^3
\end{aligned}}
\tag{25}
$$

When the chemical reaction ends, the NC and NG are exhausted simultaneously. All the products of the chemical reaction are in gaseous state. Given the universal gas constant R_0=8.31441J/mol/K, their specific gas constants (J/g/K) could be calculated as

$$
\begin{aligned}
R_{CO_2} &= \frac{R_0}{M_{CO_2}} = 0.189 J/g/K \\
R_{CO} &= \frac{R_0}{M_{CO}} = 0.2969 J/g/K \\
R_{H_2O} &= \frac{R_0}{M_{H_2O}} = 0.4619 J/g/K \\
R_{H_2} &= \frac{R_0}{M_{H_2}} = 4.1572 J/g/K \\
R_{N_2} &= \frac{R_0}{M_{N_2}} = 0.2969 J/g/K
\end{aligned}
\tag{26}
$$

Therefore, the specific gas constant of the gas mixture could be determined as

$$
\boxed{\begin{aligned}
R_{mix} &= R_{CO_2} c^*_{CO_2} + R_{CO} c^*_{CO} + R_{H_2O} c^*_{H_2O} + R_{H_2} c^*_{H_2} + R_{N_2} c^*_{N_2} \\
&= 0.3305 J/g/K
\end{aligned}}
\tag{27}
$$

The next parameter to identify is the adiabatic flame temperature T_a of the gas mixture. By looking up the specific heat at constant pressure for all its components (i.e., $c_p^{CO_2}(T)$, $c_p^{CO}(T)$, $c_p^{H_2O}(T)$, $c_p^{H_2}(T)$, $c_p^{N_2}(T)$, and $c_p^{H_2O}(T)$) from the Jannaf tables of thermochemical properties[33], the specific heat of the gas mixture at constant pressure could be evaluated as a function of temperature numerically

$$
\begin{aligned}
c_{pmix}(T) &= c^*_{CO_2} c_p^{CO_2}(T) + c^*_{CO} c_p^{CO}(T) \\
&+ c^*_{H_2O} c_p^{H_2O}(T) + c^*_{H_2} c_p^{H_2}(T) + c^*_{N_2} c_p^{N_2}(T)
\end{aligned}
\tag{28}
$$

Thus, the specific heat of the gas mixture at constant volume is

$$
c_{vmix}(T) = c_{pmix}(T) - R_{mix} \tag{29}
$$

Therefore, the adiabatic flame temperature T_a could be implicitly determined by solving the integral equation numerically

$$\boxed{Q=\int_{T_0}^{T_{a,v}} c_{vmix}dT \Rightarrow T_a = 3385.6K} \tag{30}$$

where $T_0 = 298K$ is the room temperature，Q=1000cal/g=4.1858kJ/g is the specific reaction heat given in Eq. (19). The mean specific heat at constant volume is evaluated as

$$\boxed{\overline{c}_{vmix} = \frac{4185.8J/g}{3385.6K - 298K} = 1.3557J/g/K} \tag{31}$$

For the burning rate index, a linear law (i.e., $\alpha = 1$) is adopted [34]. To further estimate the burning rate coefficient β of a specific propellant, either closed vessel tests or gun firing tests are required[35]. Herein, we adopt the data from the 7.62mm shooting experiments[36], where the mass of bullet is $m_{bullet} = 9.5g$, the mass of DBP is $m_s = 2.8g$, the combustion chamber volume is $V_0 = 3.26cm^3$, the barrel cross-section is $A = 0.456cm^2$, the barrel length is $L = 66.0cm$, and the grain size is $D_{web} = 550\mu m$. We consider the motion of a bullet in the experiments.

(1) Engraving stage before the movement of the bullet: $t \in [0, t_1]$

The critical PFF could be solved as

$$p_{cr} = \phi_{cr}\rho_0 R_{mix} T_a \tag{32}$$

where the critical engraving pressure is known from experiments.

(2) Propelling stage before the exit of the bullet at the muzzle: $t \in [t_1, t_2]$

In this stage, the displacement of the bullet x obeys

$$m_{bullet}\ddot{x} = pA \tag{33}$$

The average pressure in the combustion room (chamber and barrel behind the bullet)

could be evaluated per Eq. (18) as

$$p = \frac{\phi \rho_0 R_{mix} T_a}{J} \tag{34}$$

where the volume ratio is evaluated as

$$J = \frac{V_0 + Ax}{V_0} \tag{35}$$

Combining Eq. (7) and Eq. (33), a system of ODEs could be established. By fitting to the experimental data, one obtains the burning rate coefficient

$$\boxed{\begin{aligned} \alpha &= 1.0 \\ \beta &= 0.19 \end{aligned}} \tag{36}$$

The **Fig.1 (a)** shows the fitting result. To validate the parameters, we use another set of experimental data from a 5.8mm shooting experiment done by the No. 208 Research Institute of China Ordnance Industries. In the experiment, the mass of bullet is $m_{bullet} = 4.35g$, the mass of DBP is $m_s = 1.7g$, the combustion chamber volume is $V_0 = 1.97cm^3$, the barrel cross-section is $A = 0.2642cm^2$, the barrel length is $L = 43.3cm$, and the grain size is $D_{web} = 550\mu m$. The result shown in **Fig.1 (b)** indicates the values in Eq. (36) are reasonable.

3. Interior Ballistic Simulation of a Gun with a Gas-operated Piston System

In this section, we present the interior ballistic simulation of a gun with a gas-operated piston system based on the constitutive model of the DBP combustion gas mixture introduced in **Section 2**. Since the interior ballistic a process takes place within a

very short time, an adiabatic condition is assumed. Noteworthy, this approach could be readily applied to test the designs of other ballistic components or devices.

The 3D design of the gun is shown in **Fig.2 (a)**. It mainly comprises two parts: a 5.8mm caliber barrel with a gas room and a gas-driven rotating block mechanism to automatically fulfill bullet loading and cartridge unloading. A cutaway view of the gun is shown in **Fig.2 (b)**, where we mark two locations for testing barrel pressure and gas room pressure, respectively. In addition, we choose the radius of the gas port as a design parameter (taking values of 1.2mm, 1.4mm, and 1.6mm) and investigate its effect on the interior ballistic performance of these designs. Corresponding 3D models are created by a parametric finite element modeling technique that is capable of modify the design parameter by writing Python scripts. **Fig.3 (a)** and **Fig.3 (b)** show the components of gas-driven rotating block mechanism: a recoil spring, a guide shell, an ejector, a bolt, and a bolt carrier.

The recoil spring has a stiffness 1N/mm, and is pre-loaded by a 15N compressive force in the blocking state. The bullet is made of copper. All the other parts are made of steel. The mass of bullet is $m_{bullet} = 4.35g$, the mass of DBP is $m_s = 1.7g$, the cartridge volume is $V_0 = 1.97cm^3$, the barrel cross-section is $A = 0.2642cm^2$, the barrel length is $L = 43.3cm$. These parameters are the same with that of the 5.8mm shooting experiment. **Fig.4 (a)** shows the assembly of the barrel and the gas room. **Fig.4 (b)** shows the

assembly of the gas-driven rotating block mechanism and the bullet. The detailed design of the guide shell, the bolt, and the bullet with a cartridge are shown in **Fig.4 (c-e)**, respectively. All these parts are meshed with 8-node bricks (C3D8R element type). The ABAQUS explicit-dynamics solver to simulate the interior ballistic process, since it offers an interface for user-defined subroutines and Euler element type for fluid solid interaction (FSI) analysis based on a CEL technique. Thus, constitutive model introduced in **Section 2.3** is coded into a VUEOS subroutine that can be called by the solver. For simplicity, the rifling of the barrel is neglected and the rigid body assumption is applied to all the Lagrange parts. Additionally, the ignition of the propellant accounting for the engraving of the bullet is implemented by specifying a critical initial pressure that is equal to the engraving pressure (~150MPa) as indicated by Eq. (32).

To visualize the simulation result, **Fig.5** sequentially shows the time-history of the interior ballistic process and the pressure evolution inside the barrel and gas room within the 3 millisecond for the gas port radius 1.4mm. We further study the pressure evolution inside the barrel and gas room for designs of 3 different gas port radiuses (i.e., 1.2mm, 1.4mm, and 1.6mm respectively). **Fig.6 (a)** shows the barrel pressure-time curves (peak pressure~350Mpa) overlap before the combustion gas reaches the gas room. A larger gas port radius indicates a faster decrease of the barrel pressure. **Fig.6 (b)** shows the gas room pressure-time curves (peak pressure~50MPa, 70MPa, 80Mpa, respectively). The larger

the gas port radius, the larger the peak pressure and the faster the exit of the piston from the gas room. A sudden drop of pressure occurs due to the complete exit of the piston in the 3rd millisecond. **Fig.6 (c) and Fig.6 (d)** shows the displacement-time curves and velocity-time curves of the bullet during the 1st millisecond. Overlapping of all these curves indicate the gas-operation system affects the interior ballistic process little for the three designs. As computed, the bullet exit time is around 870μs and the muzzle velocity is 880m/s. These values are in the reasonable range of experimental observations.

4. Concluding remarks

In this paper, an approach to simulating the interior ballistic process of a gun with a gas-piston system is proposed based on a new constitutive model of the gas mixture generated by the combustion of solid propellant, and the coupled Euler-Lagrange technique for tackling fluid-solid interaction. In the approach, estimation of the material parameters of DBP is presented and validated by experiments. The result agrees well with the experimental data. The constitutive model of DBP is then incorporated into a FEA package to simulate the interior ballistic process corresponding to gun designs with different gas port radiuses. The interior ballistic parameters like the muzzle velocity and the highest barrel pressure are computed. Results show that these designs of gas ports influence the interior ballistic parameters very little. In addition, a larger gas port radius results in a larger gas room pressure, which indicates a faster operation of the

gas-operated piston.

Acknowledgement

YHJ thanks the QM project for financial support.

YHJ thanks the assistance from the No.208 Institute of China Ordnance Industry.

Competing interests

Author declares that they have no competing interests.

References

1. Ingalls, J.M., *Interior ballistics*. 1912: Wiley.
2. Krier, H. and M. Summerfield, *Interior ballistics of guns.* Progress in astronautics and aeronautics, 1979. **66**.
3. Carlucci, D.E., *Ballistics: theory and design of guns and ammunition*. 2007: Crc Press.
4. Ongaro, F., et al., *Modelling of internal ballistics of gun systems: A review.* Defence Technology, 2024. **41**: p. 35-58.
5. Kneubuehl, B.P., *Ballistics: Theory and Practice*. 2024: Springer Nature.
6. Anderson, R.D. and K.D. Fickie, *IBHVG2 (Interior Ballistics of High Velocity Guns, Version 2)--A User's Guide*. 1987.
7. Ray, S.E., M.J. Nusca, and J.F. Newill, *A Study of Projectile Response to Ballistics Environment*. 2005: Army Research Laboratory.
8. Della Pieta, P. and C. Reynard. *Numerical investigation for modeling interior ballistics two-phase flow*. in *Proceedings of the European Forum on Ballistics of Projectiles*. 2000.
9. Gough, P.S., *Interior ballistics modeling: extensions to the one-dimensional XKTC code and analytical studies of pressure gradient for lumped parameter codes*. 2001.
10. Miner, R., *Computational interior ballistics modeling.* 2013.
11. Ray, S.E. and T.E. Tezduyar, *Fluid–object interactions in interior ballistics.* Computer Methods in Applied Mechanics and Engineering, 2000. **190**(3-4): p. 363-372.
12. Şentürk, A., H. Işık, and C. Evci, *Thermo-mechanically coupled thermal and stress analysis of interior ballistics problem.* International Journal of Thermal Sciences, 2016. **104**: p. 39-53.
13. Uyanık, M.S., et al., *Design, analysis, manufacturing, and testing of a composite gun barrel.* Polymer Composites, 2024. **45**(13): p. 11804-11815.
14. Deng, S., et al., *Interior ballistics analysis of shotgun using discrete element method.* Finite Elements in Analysis and Design, 2022. **201**: p. 103698.
15. Cheng, C. and X. Zhang, *Modeling of interior ballistic gas-solid flow using a coupled computational fluid dynamics-discrete element method.* Journal of Applied Mechanics, 2013. **80**(3).
16. Jang, J.-S., S.-H. Oh, and T.-S. Roh, *Development of three-dimensional numerical model for combustion-flow in interior ballistics.* Journal of Mechanical Science and Technology, 2016. **30**(4): p. 1631-1637.
17. Han, S., et al. *ALE-Based FSI simulation of solid propellant rocket interior*. in

48th AIAA Aerospace Sciences Meeting Including the New Horizons Forum and Aerospace Exposition. 2010.

18. Oñate, E., et al., *The particle finite element method—an overview.* International Journal of Computational Methods, 2004. **1**(02): p. 267-307.
19. Messahel, R. and M. Souli, *SPH and ALE formulations for fluid structure coupling.* CMES-Computer Modeling in Engineering and Sciences, 2013. **96**.
20. Long, T., et al., *An arbitrary boundary with ghost particles incorporated in coupled FEM–SPH model for FSI problems.* Journal of Computational Physics, 2017. **350**: p. 166-183.
21. Noh, W.F., *CEL: A time-dependent, two-space-dimensional, coupled Eulerian-Lagrange code*. 1963, Lawrence Livermore National Lab.(LLNL), Livermore, CA (United States).
22. Abaqus, D., *ABAQUS online documentation.* Providence, RI, USA: Dassault Systemes Simulia Corporation, 2016.
23. Wolf, K., et al., *MpCCI: Neutral interfaces for multiphysics simulations*, in *Scientific Computing and Algorithms in Industrial Simulations: Projects and Products of Fraunhofer SCAI*. 2017, Springer. p. 135-151.
24. Matsson, J.E., *An introduction to ANSYS fluent 2022*. 2022: Sdc Publications.
25. Truesdell, C., *Historical introit the origins of rational thermodynamics*, in *Rational thermodynamics*. 1984, Springer. p. 1-48.
26. Eisenreich, N., T. Fischer, and G. Langer. *Burning rate models of gun propellants*. in *Proceedings of the European Forum on Ballistics of Projectiles*. 2000.
27. Struble, R.A., *A study of the interior ballistic equations.* Archive for Rational Mechanics and Analysis, 1959. **3**(1): p. 397-416.
28. Miura, H. and A. Matsuo. *Numerical simulation of solid propellant combustion in a gun chamber*. in *42nd AIAA/ASME/SAE/ASEE Joint Propulsion Conference & Exhibit*. 2006.
29. Iorga, O., et al., *Theoretical and experimental determination of interior ballistic parameters of recoilless gun.* UPB Sci Bull, Ser D: Mech Eng., 2021. **83**: p. 2021.
30. Bizot, A. and M. Beckstead. *A model for double base propellant combustion*. in *Symposium (international) on combustion*. 1989. Elsevier.
31. Boulkadid, K.M., et al., *Estimation of the ballistic parameters of double base gun propellants.* Propellants, Explosives, Pyrotechnics, 2020. **45**(5): p. 751-758.
32. Grossman, B., *Fundamental concepts of real gasdynamics.* Virginia Polytechnic Institute and State University: Blacksburg, VA, USA, 2000.
33. Stull, D.R., *JANAF Thermochemical Tables*. Vol. 1. 1965: Clearinghouse.
34. Lengellé, G., J. Duterque, and J. Trubert, *Combustion of solid propellants*. 2002, DTIC Document.

35. Gupta, G., et al., *Various methods for the determination of the burning rates of solid propellants: an overview.* Central European Journal of Energetic Materials, 2015. **12**(3): p. 593-620.
36. Değirmenci, E., et al., *Thermo-mechanical analysis of double base propellant combustion in a barrel.* Applied Thermal Engineering, 2016. **102**: p. 1287-1299.

Fig. 1

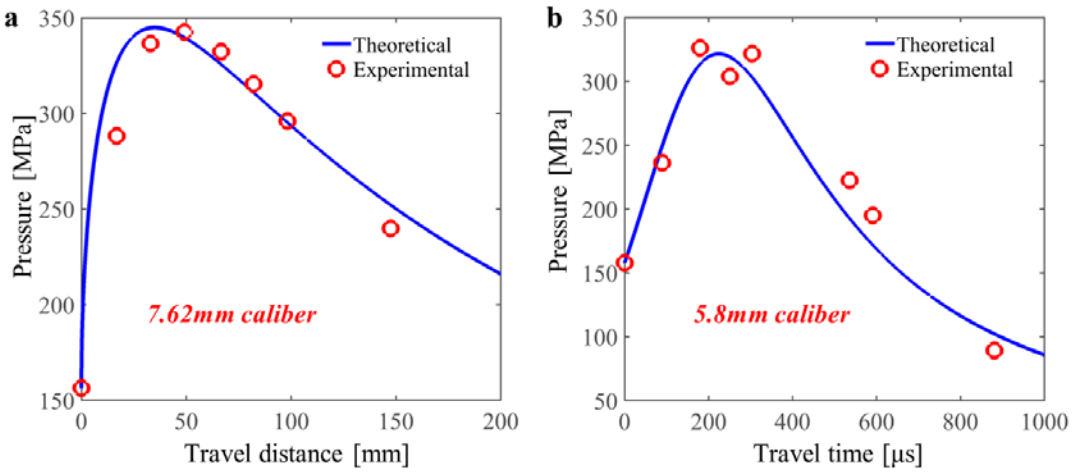

(a) Pressure-distance curve and experimental data **(b)** Pressure-time curve and experimental data

Fig. 2

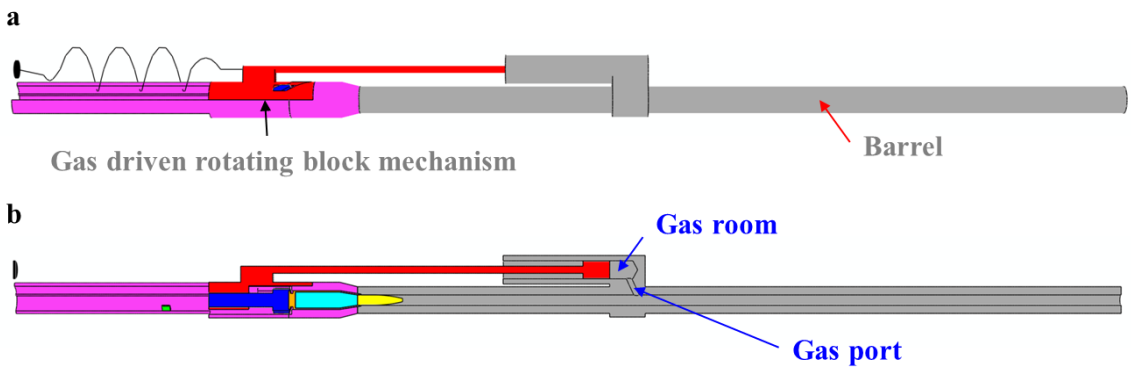

(a) A schematic showing the main components of a gun: Barrel, Gas room, and Gas driven rotating block mechanism **(b)** Cutaway view of the gun

Fig. 3

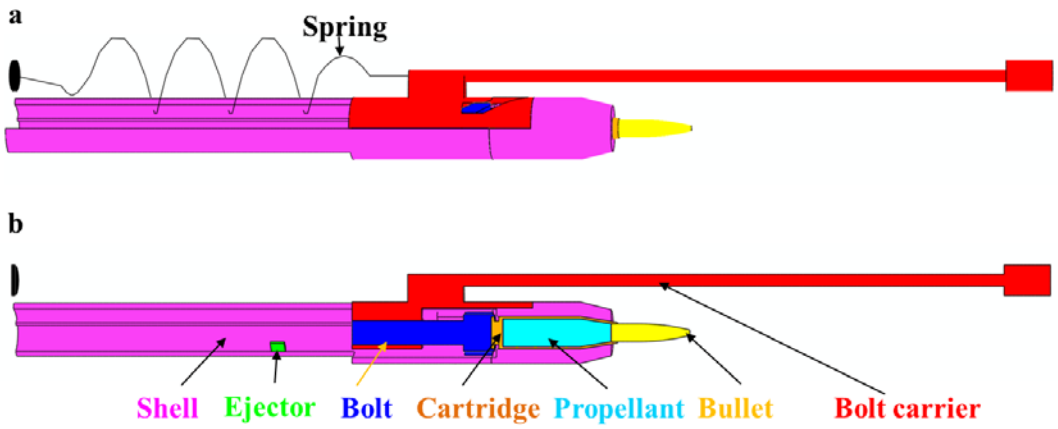

(a) A schematic showing the Gas driven rotating block mechanism **(b)** Cutaway view of the mechanism with bullet inside showing the components: Bold carrier, Bolt, Ejector, and Guide shell.

Fig. 4

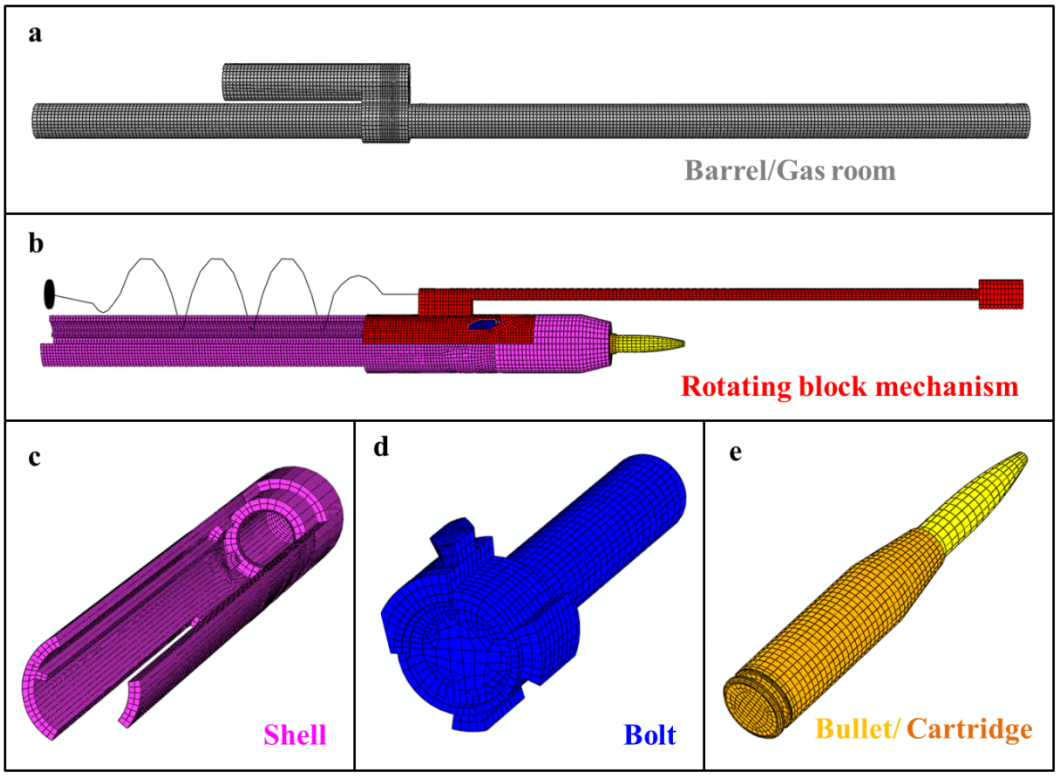

(a) Assembly of the barrel and gas room with a mesh**(b)** Assembly of the gas driven rotating block mechanism and bullet with a mesh **(c)** Design and mesh of shell **(d)** Design and mesh of the bolt **(e)** Design and mesh of the bullet and cartridge

Fig. 5

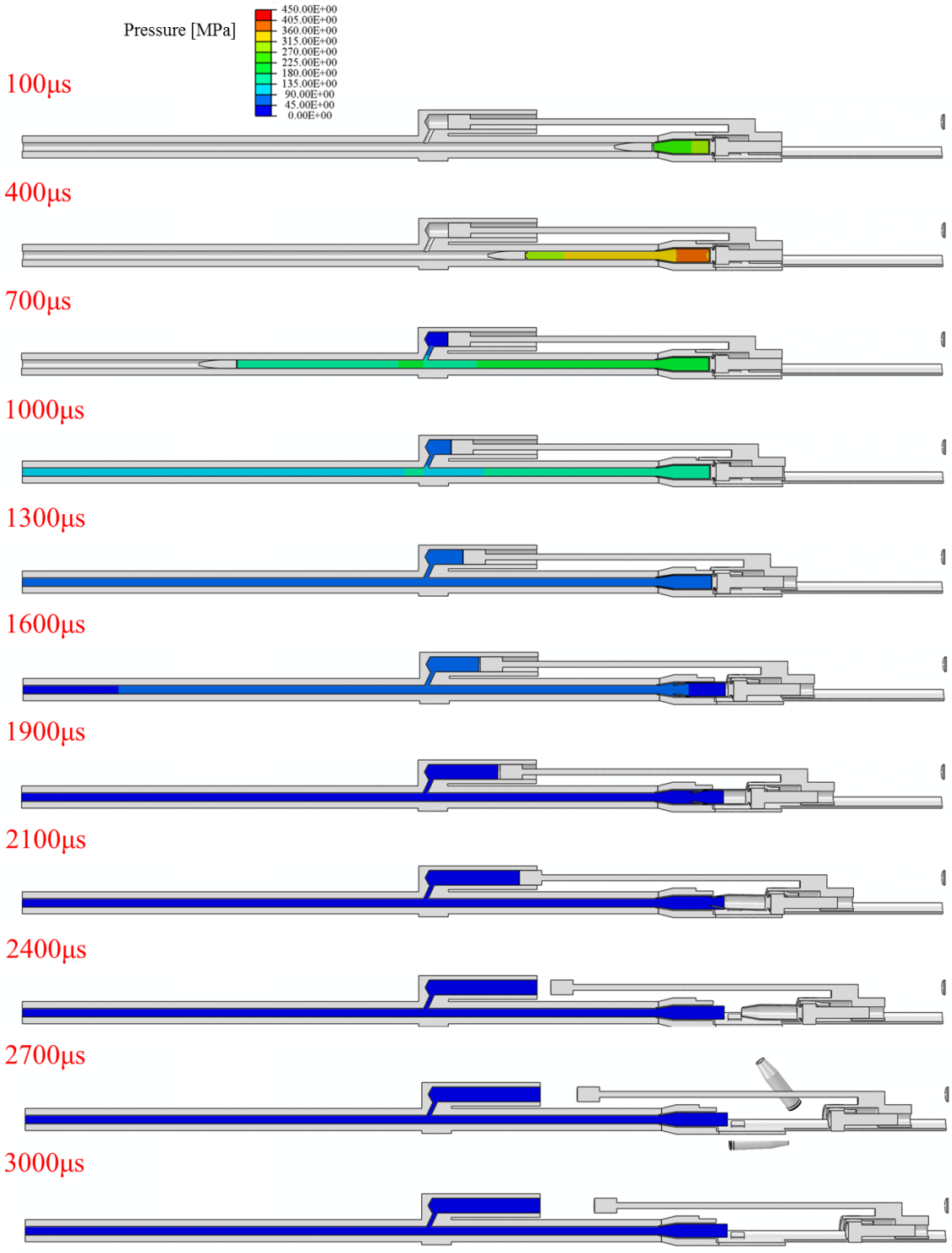

Time-history diagram showing the interior ballistic process and pressure evolution inside the barrel and the gas room within 0μs~3000μs (gas port radius=1.4mm)

Fig. 6

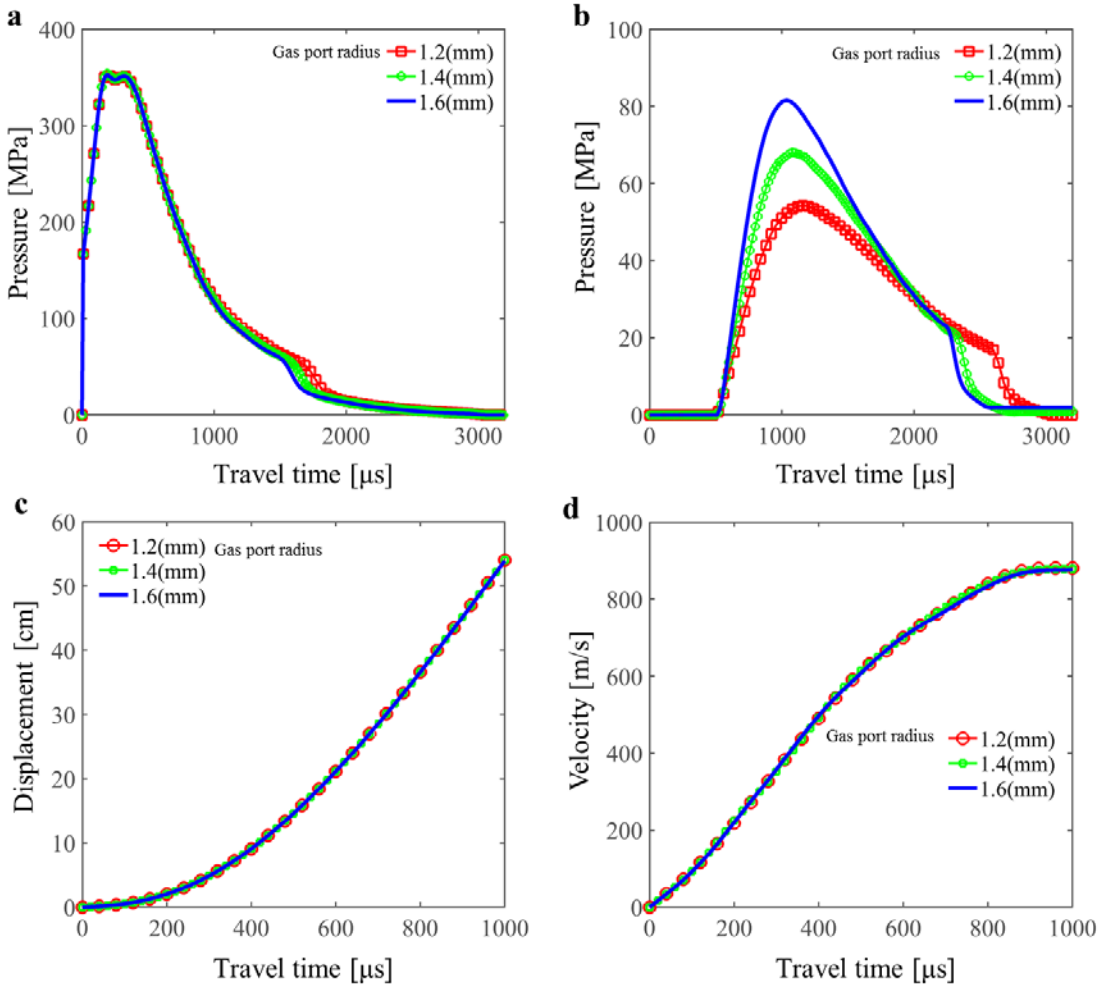

(a) Barrel pressure-time curves **(b)** Gas room pressure-time curves **(c)** Bullet displacement-time curves **(d)** Bullet velocity-time curves